Look, Evolve and Mold: Learning 3D Shape Manifold via Single-view Synthetic Data

Qianyu Feng[1], Yawei Luo[2], Keyang Luo[3], Yi Yang[1]

[1]ReLER, AAII, University of Technology Sydney
[2]Zhejiang University [3]Huazhong University of Science and Technology

Abstract

*With daily observation and prior knowledge, it is easy for us human to infer the stereo structure via a single view. However, to equip the deep models with such ability usually requires abundant supervision. It is promising that without the elaborated 3D annotation, we can simply profit from the synthetic data, where pairwise ground-truth is easy to access. Nevertheless, the domain gap is not neglectable considering the variant texture, shape and context. To overcome these difficulties, we propose a domain-adaptive network for single-view 3D reconstruction, dubbed **LEM**, to generalize towards the natural scenario by fulfilling several aspects: (1) **Look**: incorporating spatial structure from the single view to enhance the representation; (2) **Evolve**: leveraging the semantic information with unsupervised contrastive mapping recurring to the shape priors; (3) **Mold**: transforming into the desired stereo manifold with discernment and semantic knowledge. Extensive experiments on several benchmarks demonstrate the effectiveness and robustness of the proposed method, LEM, in learning the 3D shape manifold from the synthetic data via a single-view.*

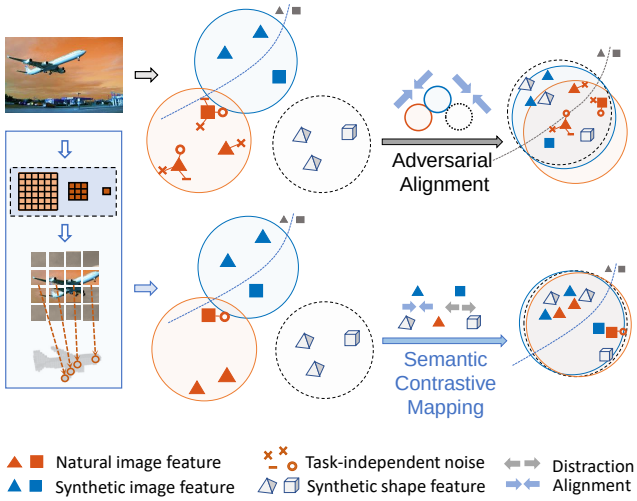

Figure 1. This task aims to reconstruct a 3D shape from a natural image. The top row shows the traditional domain-wise alignment pipeline which results in the misalignment. The bottom row illustrates the proposed LEM. First, it *'Look'* at the image with multi-scaled structured attention to equip the representation with local information. Then, it *'Evolve'* by leveraging the contrastive mapping which assists to maintain a better marginal distribution via the semantic knowledge. Thus, LEM can favourably *'Mold'* the target object with robustness and expressiveness.

1. Introduction

By virtue of spatial imagination, perceiving the volumetric shape with a single view is trivial for human. The allied vision task is formed as single-view 3D reconstruction [7, 17, 50], which attracts considerable attention due to the increasing demand for different 3D applications such as navigation, robotic operation and autonomous driving. Nevertheless, it remains a challenging task for intelligent systems to match such ability without sufficient knowledge priors. To tackle this problem, traditional methods rely on a variety of puissant visual cues like shading [20], texture [9] or vanishing point [21]. With the surge of interest in learning-based reconstruction methods, a straightforward solution is to introduce explicit 3D supervision, such as ground-truth voxel, mesh or point cloud of the target object. With abundant supervision, current deep learning methods are capable of learning different priors [36, 38], thus boosting the reconstruction performance. Notwithstanding decent progress gained by the fully-supervised methods [8, 15], such success is at the considerable price of dense annotations by cumbersome labors. A remedy for this would be resorting to synthetic data, such as CAD models, which has a large amount of 3D data paired with high-quality annotations [4]. Nonetheless, the reconstruction models trained on synthetic data usually perform sub-optimally in real scenarios. The gap lies in the domain shift between natural images and synthetic data with different textures, shapes and noisy background.

To tackle the domain shift, recent research works have

devised and incorporated domain adaptation techniques to mitigate the performance drop in the target domain [1, 31]. Generally, these methods aim to learn representation indistinguishable for different domains by aligning the domain distributions [30, 34]. Although achieving impressive progress in addressing domain adaptation tasks [46, 31], the performance is limited for cross-domain 3D reconstruction.

Merely narrowing the gap between the distribution across domains neglects the existence of nuisance factors from the real scenario. Beyond that, current methods tend to extract high entangled embeddings and fail in learning the local structure details, e.g., missing the armrests of "chair". Moreover, it is misleading for models to roughly align the domain-wise marginal distribution while ignoring the inherited semantic information. The knowledge confusion caused by the global alignment results in the catastrophic destruction in the categorical distribution, such as aligning the image feature of a "plane" to the shape of a "car" in the manifold space by force. Accordingly, to overcome the gap between synthetic data and real scenes with various texture, shape and context, we propose to first leverage the local structure to enhance the representation via **'look'** with a *Spatial Structured Attention (SSA)* module, encoding both the structure information and partial dependencies. It also benefits in filtering out unrelated information from the context. Furthermore, the semantic information is leveraged with a *Contrastive Semantic Mapping (CSM)* module for semantically aligning the domain gap. Different from previous approaches, CSM can semantically **'evolve'** the representation of the target from a single view to the corresponding shape prior without relying on the category labels. It aligns the image feature with the corresponding shape prior by exploiting the visual similarity. Lastly, with the expressive structure information and semantic knowledge, LEM achieves to **'mold'** the desired shape from the 3D manifold. To sum up, the contributions of our work are listed as follows:

- We propose a novel method for 3D reconstruction from synthetic data, named LEM, by leveraging the spatial structured attention on the locality and removing the noneffective noise, which is orthogonal to the previous efforts focusing on the alignment at the global scope.
- Leveraging the semantic knowledge, we discover that LEM is better generalized into the real scene and largely closes the gap between synthetic data and natural targets in an unsupervised style.
- We further demonstrate that LEM performs well in the real world with extensive experiments and competitive results on several benchmarks which proves the effectiveness and robustness of the proposed method.

2. Related Work

Single-view 3D Reconstruction. Many data-driven learning approaches have been introduced to estimate the 3D shape from a single image. Based on the data format, these methods are categorized into three classes: voxel-based, point-based and mesh-based. The voxel-based methods [7, 17, 50, 44, 22, 54] usually manipulate the voxel grids based on 3D convolution neural network directly. Owing to the requirements of computing resources, these approaches are merely capable of handling voxel grids with a relatively small resolution and fail in capturing the shape details. To relieve such a problem, recently, some works [36, 38, 55, 6] aim to estimate the truncated signed distance fields to preserve more details. Point-based [12, 35, 19] approaches regress point clouds from a single image to represent the corresponding object or scene directly. Both voxel-based and point-based methods require implicit surface reconstruction methods to generate the final triangle mesh. The above methods require ground-truth 3D models, which are difficult to obtain for real scenes. To relieve this problem, Pinheiro *et al.* [39] introduce a domain confusion reconstruction method How to effectively fulfill the 3D reconstruction across domains is still an open problem.

Domain Adaptation for 3D Reconstruction. Domain adaptation aims to mitigate the performance drop when transferring a model from source to target domain. As suggested by Ben-David [1], at the core of domain adaptation is to reduce the domain divergence. In this spirit, domain adaption can be approached by either aligning distribution between domains [31, 34, 14], synthesizing labeled target samples [27, 41, 33] or estimating pseudo label in target domain [56, 28, 47]. However, these methods are demonstrated to be harmful to the feature discriminability [5, 30] thus damaging the class-level information, which may lead to misalignment and poor generalization performance.

Self-supervised Models. A recent trend has introduced the self-supervised learning idea to the traditional adversarial methods [26, 42] to enhance the feature discriminability. For example, contrastive learning suggests narrowing the positive pairs while pushing apart the negative pairs in the feature space, thus help the same semantics to be clustered in the manifold space. Comparing to the thriving development of domain adaptation technologies for 2D tasks such as image classification [5] and segmentation [32], less progress has been made towards a 3D scenario. To name a few, Qin *et al.* [40] proposed PointDAN to align 3D point cloud representation between CAD model and scanned data. Cao *et al.* [3] transformed the 3D animal pose knowledge from labeled to unlabeled animal classes. Back to our main concern, to the best of our knowledge, Pedro *et al.* [39] have made the first attempt towards the domain adaptive single-view 3D reconstruction task. In their seminal work, they used adversarial learning to align synthetic

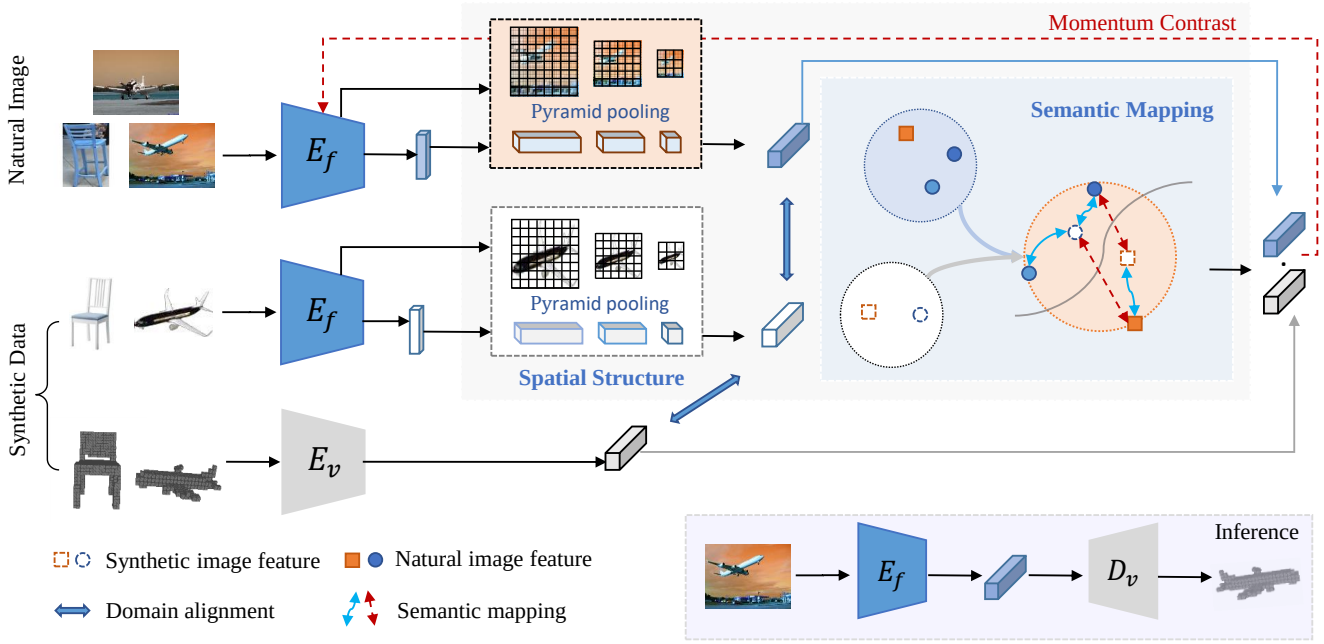

Figure 2. The conceptual architecture of the proposed LEM method for domain-adaptive single-view 3D reconstruction. We approach this task with two main modules: **(a) Spatial Structured Attention (SSA)** aims to enrich the latent representation of the image by learning the local structure and the non-local dependencies at the pixel-level; **(b) Contrastive Semantic Mapping (CSM)** is responsible for semantically mapping the 2D representation with the 3D shape priors via contrastive learning which better aligns the domain difference while keeps the semantic distribution at the instance-level.

and real domains but neglect learning the structure of the object.

3. Method

3.1. Single-view 3D Reconstruction

Given a natural image $\boldsymbol{x}^n \in \mathcal{X}$, the target of this problem is to reconstruct a volumetric shape $\boldsymbol{v}^n \in \mathcal{V}$ for the target object. Only the synthetic 2D images with their corresponding 3D models, as well as the natural 2D images are accessible during training. Different from the synthetic paired image and volumetric shape $\{\boldsymbol{x}_i^r, \boldsymbol{v}_i^r\}_{i=1}^{N_r}$, the unlabeled natural images, $\{\boldsymbol{x}_j^n\}_{j=1}^{N_n}$, are sampled from a different distribution $\mathcal{D}_n(\boldsymbol{x}, \boldsymbol{v})$ in the real world. The key challenges consist of two main aspects: the distribution gap between the synthetic data and the real world, as well as the gap existing in the different manifolds of 2D images and 3D shapes with inconsistent appearance and manifold distribution. From this perspective, it is desirable to learn such representation that meets the following sub-goals: (1) the adaptive alignment from the embedding of 2D image and the desired 3D shape; (2) the alignment of the embeddings of natural images with the rendered images from synthetic data; (3) the reconstruction of the volumetric shape from the embeddings of the natural images.

Primarily, the architecture of our method is based on an auto-encoder for 3D reconstruction via an encoder E_f fed with an image and a decoder D_v outputs a stereo shape. The overall framework is illustrated in Figure 2. Towards this, numerous CAD objects are accessible during training as data samples from the source domain. Rendered images paired with the volumetric representation are drawn from the distribution of the synthetic data. To be specific, a volumetric encoder E_v is first pretrained together with D_v in the source domain to learn the shape prior knowledge. The parameters of the volumetric encoder and decoder are fixed after the pretrain to maintain the prior knowledge from the shape manifold. The encoder E_f maps an image into a low-dimensional embedding representation $e \in \mathcal{E} \subset \mathbb{R}^{d_e}$. Then, the decoder D_v maps the manifold in the latent space back to a 3D shape representation. Since the shape auto-encoder is trained with true 3D shapes, the learned embeddings from the encoder E_v lie in the shape *manifold* $\mathcal{E}$, containing compact embeddings of volumetric shapes. With the prior knowledge acquired in the source domain, the shape prior information is implicitly encoded in the rich representation *manifold*. It is worth mentioning that the model is trained with only the natural images during training while the ground-truth shapes are only for evaluation. While at inference time, only the reconstruction network is functioning to predict the voxel shape given a natural image from the target domain. The image encoder E_f embeds an image into a high-level manifold ξ from which the volumetric decoder D_v reconstructs the stereo shape.

Targeting on the aforementioned challenges, the proposed method, LEM, aligns the representation from both the fine-grained pixel-level and the instance-level: (i) *Spatial Structured Attention* (SSA) module, which is responsible for learning a rich latent representation by leveraging the local structure and the non-local dependencies at multiple scales; (ii) *Contrastive Semantic Mapping* (CSM) module, in charge of semantically mapping the representation with the 3D shape priors by contrastive learning. The overview of the proposed method is illustrated in Figure 2 with the mentioned modules embedded into the auto-encoder architecture.

3.2. Spatial Structured Attention

Non-local Structure. We first propose to leverage the local structure from an image $\boldsymbol{x} \in \mathbb{R}^{C\times H\times W}$ which can better focus on the target region and learns the local structure of the object. We apply different 1×1 convolutions to transform the encoded feature of the input image $\boldsymbol{x}$ to different embeddings, which also resize the channel number to $\hat{C}$. With a flattening operation, these embeddings are resized into $\boldsymbol{x}_k, \boldsymbol{x}_v, \boldsymbol{x}_q$ with shape $\hat{C} \times N$, where $N = H \cdot W$ represents the number of the local parts. Then, the similarity matrix $\gamma \in \mathbb{R}^{N\times N}$ is calculated by a matrix multiplication. By referring to the non-local block [48], the final output is calculated as:

$$\hat{\boldsymbol{x}} = Concat(W_m(\boldsymbol{x}_v \cdot \mathrm{Softmax}(\boldsymbol{x}_k^{\mathrm{T}} \cdot \boldsymbol{x}_q), \boldsymbol{x})), \quad (1)$$

where W_m is applied to adjust the weight of the non-local output against the input $\boldsymbol{x}$ with a 1×1 convolution layer. It also recovers the channel dimension from $\hat{C}$ back to C.

Pyramid Pooling. Inspired by previous works [29, 48] which leverage the multi-scale context features to boost the local structure and the dependencies learning, we hereby adopt the Spatial Pyramid Pooling [23] containing several pooling layers with multiple output sizes in parallel, which is also parameter-free and computing-efficient. Therefore, we incorporate the multi-scale pooling with the non-local module to enhance the richness and distinctiveness of the information in the embedding manifolds. The non-local module is effective in capturing the dependencies across different parts. However, such operation is both time and memory-consuming compared to normal convolutions in the deep neural network.

Thus, we further rescale the image features at a lower stage from the backbone network into multiple scales to acquire a richer representation with knowledge from structures at different scales. This can be realized on the condition of changing N to a smaller dimension, and keeping the same output size $\hat{C}$. In the meantime, the computational complexity could be considerably decreased compared to the full scale. With the adaptive pooling $\mathcal{P}$, the context features are re-scaled into multiple sizes to sample contextual points denoted as $\boldsymbol{x}_c \in \mathbb{R}^{\hat{C}\times S}$, where S is the number of sampled anchors, calculated by:

$$\boldsymbol{x}_c = \mathcal{P}(\boldsymbol{x}), \quad (2)$$

$$M = \mathrm{Softmax}(\boldsymbol{x}_e^{\mathrm{T}} \cdot \boldsymbol{x}_c), \quad (3)$$

where M denotes the similarity matrix between the output feature $\boldsymbol{x}_e$ of the image encoder and its context feature $\boldsymbol{x}_c$. Following non-local blocks, the final output x_o is calculated with the attended features $\hat{\boldsymbol{x}}_c$ from the context features:

$$\hat{\boldsymbol{x}}_c = M \cdot {\boldsymbol{x}_c}^{\mathrm{T}}, \quad (4)$$

$$\hat{\boldsymbol{x}} = \mathrm{Concat}(W_o({\hat{\boldsymbol{x}}_c}^{\mathrm{T}}), \boldsymbol{x}_e). \quad (5)$$

Moreover, the spatial structured attention provides sufficient statistics about the global semantic cues to remedy the potential performance deterioration caused by the noise from the real scenario.

3.3. Semantic Contrastive Mapping

Previous works only focus on narrowing the domain gap with all samples might lead to catastrophic misleading results as the categories in the source and target domain are not always consistent. All samples from different categories are aligned together due to the ignorance of the semantic information. Furthermore, there also exists ambiguity with multiple explanations from a single-view image. To tackle this, we propose to exploit the semantic mapping of the samples with priors from the source domain.

Given a natural image $\boldsymbol{x}^n$, we aim to leverage the semantic information in the image/voxel pair from the synthetic data. The shape of the synthetic data $\boldsymbol{v}^r$ is considered as a positive sample for $\boldsymbol{x}^n$ if they are from the same category, otherwise, $\boldsymbol{v}^r$ is regarded as a negative sample. The objective is to align the natural image $\boldsymbol{x}^n$ and the volumetric shape $\boldsymbol{v}^r$ conditioned on the semantic information of the category. Contrastive Semantic Mapping module functions in an unsupervised mechanism by leveraging the similarity between the embedded representation of the synthetic image and the real image as semantic supervision:

$$s(\boldsymbol{x}^r, \boldsymbol{x}^n) = \sigma(dist(E_f(\boldsymbol{x}^r), E_f(\boldsymbol{x}^n))), \quad (6)$$

where σ is a sigmoid function for normalization.Empirically, we apply the *l2-norm* metric which can better measure the visual distance. The pseudo semantic label p_s for the pair of $\boldsymbol{x}^r, \boldsymbol{x}^n$ is valued as 1 if $s(\boldsymbol{x}^r, \boldsymbol{x}^n) \leqslant 0.5$ else set to 0. Then, we learn the similarity between the natural image $\boldsymbol{x}^n$ and the volumetric shape $\boldsymbol{v}^r$ with a linear transformation:

$$a(\boldsymbol{x}^n, \boldsymbol{v}^r) = \sigma(W_a\,\mathrm{Concat}(W_m\boldsymbol{x}^n, W_n\boldsymbol{v}^r)), \quad (7)$$

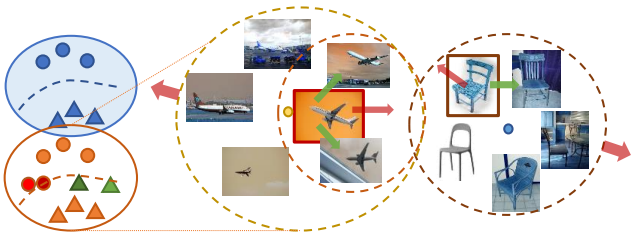

Figure 3. Illustration of Contrastive Semantic Mapping at the instance level. Samples are rearranged in the representation manifold according to the visual similarity to enhance the semantic distribution of samples.

where W_a, W_m, W_n are parameters to be learned, σ is a sigmoid function for the normalization of the similarity score. Optimized with CSM, the constraint is defined as:

$$\mathcal{L}_{CSM} = -\sum_{i=1}^{K} \log \frac{\exp\left(a(\boldsymbol{x}_i^n, \boldsymbol{v}_i^r)/\tau\right)}{\sum_{j=1}^{M} \exp\left(a(\boldsymbol{x}_j^n, \boldsymbol{v}_j^r)/\tau\right)}, \quad (8)$$

where τ is a scalar temperature parameter. K is the number of positive samples $\boldsymbol{v}^r$ for $\boldsymbol{x}^n$, M denotes the total number of pairs. In this way, the representation of the object from the image is semantically aligned with the shape priors with similar visual appearance.

3.4. Objectives

Overall, the goals of learning consistency in two-fold: On one hand, the encoder is trained for learning an indistinguishable representation invariant to domains. On the other hand, the learned embedding space is constrained to conform to the manifold pretrained with the shape priors from the source domain. Further on, one of the objectives is to learn an embedding manifold invariant to the data format, *e.g.*, image and 3D shape in our setting. Thus, we impose an adversarial loss to fulfill this constraint by penalizing the model if the distribution of image representations does not match the shape manifold. Based on that, a discriminator C_s parameterized by θ_s is in charge of classifying whether a sample is drawn from the image embeddings or the shape manifold. where parameters θ_s in the discriminator C_s are trained to minimize the loss. Oppositely, parameters θ_x aim to maximize it. In this way, E_f is forced to learn the embeddings from the image $\boldsymbol{x}^r$ aligned with the shape manifold of $\boldsymbol{v}^r$. E_f is also applied to extract features of the natural images.

Considering only the global alignment, it is observed that the output embeddings are not expressive enough, especially for images with noise from the background. Hence, we propose to enhance the representation with the attention mechanism for better exploiting the essential information for reconstruction. In o obtain representation invariant to the domain, we also apply the adversarial learning to map the embeddings through a minimax game between the discriminator C_d and the feature encoder E_f. The discriminator C_d, parameterized by θ_d, is designated to classify the domain of an embedded representation, which is optimized in an adversarial style.

In total, the model is optimized to learn the desired shape manifold with representations that are domain-invariant and lie in the same manifold with the shape priors. Domain confusion across the rendered images and the natural images is achieved by applying Reverse Gradient algorithm [16], which optimizes the parameters θ_x to maximize the discriminator loss directly, while θ_d minimizes that. Consequently, these two objectives are realized by optimizing the following function in an adversarial style:

$$\mathcal{L}_{Adv} = \mathcal{L}_{x\to v}(\theta_x, \theta_v) + \mathcal{L}_{n\to r}(\theta_x, \theta_d). \quad (9)$$

$$\mathcal{L} = \mathcal{L}_{Rec} + \beta\mathcal{L}_{Adv} + \lambda\mathcal{L}_{CSM}, \quad (10)$$

where β is the balance hyper-parameter for the two adversarial losses and λ is for the semantic mapping loss among the loss terms.

To sum up, the proposed LEM first exploits the information from a single-view image with the proposed Spatial

Algorithm 1 The proposed method for domain adaptive 3D reconstruction from a single view.

Require: Labeled synthetic image and voxel pairs $\{(x_i^r, v_i)\}_{i=1}^{N_s}$ as the source domain, natural images $\{x_j^n\}_{j=1}^{N_t}$ sampled from the target domain.

Ensure: Parameters θ in the auto-encoder modules: image encoder E_f, voxel encoder E_v, voxel decoder D_v and the two domain discriminators C_d, C_s

```
Pretrain the volumetric auto-encoder on {x_i, v_i}_{i=1}^{N_s}, update the parameters and freeze E_v and D_v
e = 0
while not converge do
  for iter = 1 to max_iter do
    # feature extraction from the image
    Extract multi-scale features by omni-pooling
    Calculate the attended feature with Eq. 2 and Eq. 4
    # representation mapping at the instance level
    Calculate the pair distance between synthetic rendered image x^r and natural image x^n
    # 3d shape reconstruction
    Reconstruct images by feed the extracted feature from E_f into D_v
    Train with the sampled batch by optimizing loss in Eq. 10, update parameters in E_f, C_d, C_s
    e = e + 1
  end for
end while
```

Table 1. Comparative single-view 3D reconstruction results on Pix3D measured with IoU and CD metrics. PSGN* directly adopts the ground-truth mask, while MarrNet†, DRC and ShapeHD use 2.5D sketches to guide the training. We show competitive results in both metrics without using extra information.

	IoU	CD
3D-R2N2[8]	0.136	0.239
3D-VAE-GAN [51]	0.171	0.182
PSGN* [13]	-	0.199
MarrNet† [49]	0.231	0.144
DRC† [45]	0.265	0.160
AtlasNet [18]	-	0.148
AtlasNet + mask* [18]	-	0.126
ShapeHD† [52]	0.284	0.123
DAREC [39]	0.241	0.140
LEM	**0.292**	**0.108**

Table 2. Single-view 3D reconstruction results on the categories of 'chair', 'car', 'aeroplane' in Pascal3D+. Experiments are conducted under the single-class setting by sampling data from one category from the target domain.

	chair	car	aeroplane
DAREC [39]	0.212	0.229	0.197
OSA-S	0.227	0.241	0.213
OSA-M	0.236	0.249	0.225
OSA-L	0.250	0.277	0.248
LEM	**0.264**	**0.295**	**0.262**

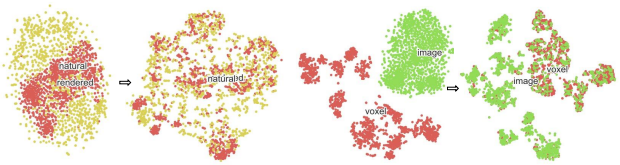

Figure 4. The distribution of the encoded embeddings of rendered images and natural images from the output of encoder E_f before and after the domain adaptation alignment.

Structured Attention module to distill the inherent knowledge such as local structure and parts dependencies, in the first step of *'Look'*. In this way, the desired representation related to the shape is extracted instead of the unrelated pixel-level noise from the background. Furthermore, Contrastive Semantic Mapping is designated to leverage the semantic information with unsupervised contrastive learning which aims to *'Evolve'* the representation of samples to the corresponded shape priors. Therefore, LEM can learn an expressive and discriminative representation to *'Mold'* the desired shape with only a single view of the object.

4. Experiment

Datasets. Similar to [39], all experiments are conducted on three datasets: ShapeNet [4], Pix3D [43] and PASCAL 3D+ [53]. The ShapeNet preprocessed by [8] is regarded as the source domain, which contains rendered images with $50k$ CAD models of 13 object categories [4]. For the target domain, Pix3D and PASCAL 3D+ are selected as two different target domains on which we conduct the inference. Pix3D is a large-scale benchmark for 3D-related tasks and the images of the chair are used widely with high diversity and variance. PASCAL 3D+ is a dataset built on PASCAL VOC 2012 [11] with 3D annotations. It contains a limited amount of 3D models which results in that objects with different shapes that might correspond to the same 3D shape. For a fair comparison, the natural images from the target domain are used without any ground truth or side information during the training. The corresponding target CAD models are for benchmarking purposes in the evaluation only.

Training. The voxel auto-encoder backbone aims to learn shape priors and capture the intrinsic shape complexity of different objects, we train the model using the ShapeNet dataset and the resolution of voxel is 32^3. The encoder E_v of this model composed of five $3 \times 3 \times 3$ 3D convolutional layers, each followed by a max-pooling (except the first layer) and ReLU [37] non-linearity. The number of hidden units are 32, 32, 64, 128 and 256 respectively. Similarly, the voxel decoder D has five $3 \times 3 \times 3$ convolution layers, but instead of max-pooling, we apply the bilinear upsampling. The dimension of the latent representation is 256. Once training converges, we freeze the parameters of the encoder and the decoder and use them in the reconstruction stage. To optimize, we used Adam [25] with learning rate of 10^{-4} and batch size of 32. The architecture of the reconstruction network is based on an encoder-decoder structure. The parameters of network E_f are initialized with a ResNet-50 [24] that was pre-trained to perform classification on ImageNet dataset [10]. We replace the classification layer with a randomly initialized layer that outputs a vector with the same dimension of the latent space. The two discriminators C_s and C_d map the embedded features to the probability of which domain the input comes from (modeled by a softmax [2]). Two fully-connected layers of dimension 1024 are adopted, followed by ReLU. To optimize, we used Adam [25] with learning rate of 10^{-4}. We follow [39] and adopt the Intersection over Union (IoU) and the Chamfer Distance (CD) as the evaluation metrics to evaluate the performance of our method quantitatively, which are commonly used evaluation metrics in single-view three-dimensional reconstruction task.

4.1. Competitive Results

During training, the reconstruction network has access to data samples from ShapeNet synthetic rendered images and ground truth labels. In the inference, the input of the model is only a single natural image while the target is to

Table 3. Single-view 3D reconstruction results on Pascal3D+. We show results on both IoU and CD metrics. Our approach only takes the accessible natural images from the target domain. WHile other methods profit from extra information during training: DRC and ShapeHD applies depth/normals/silhouettes, OGN adopts a much stronger decoder with higher resolution.

	IoU	CD	chair	car	aeroplane
3D-R2N2[8]	0.113	0.238	0.305	0.305	0.284
DRC [45]	-	0.158	0.099	0.112	0.122
OGN [44]	-	-	0.087	-	-
ShapeHD [52]	0.245	0.137	0.129	0.094	0.119
DAREC [39]	0.263	0.135	0.101	0.108	0.115
LEM	**0.349**	**0.104**	**0.110**	**0.085**	**0.109**

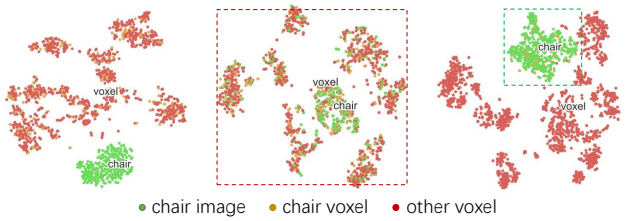

Figure 5. The distribution of the encoded embeddings of images from the output of encoder E_x and embeddings of shape voxels from the output of encoder E_v is aligned after the adversarial adaptation where the distribution of categories are kept well.

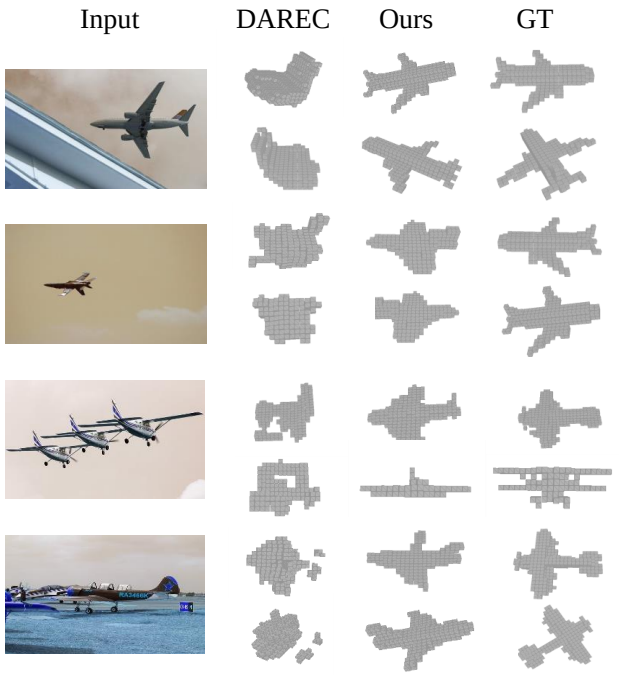

Figure 6. Reconstruction comparison of results generated by the baseline and ours against the ground truth shapes from Pascal3D+.

reconstruct a volumetric 3D model for the object in it.

Reconstruction for Pix3D dataset. Following [39], natural images from ImageNet in the category of 'chair' in *PASCAL 3D+ r1.1* are taken as target samples without using the label. Following previous works [43, 39], we evaluate our method on the 2894 untruncated and unoccluded 'chair' samples. Our LEM performs better in distinguishing the representation of the target object from the background while generating consistent and stable reconstruction results which are shown in Table 1. Our method overwhelms the other baselines by raising the IoU by 15.8% and CD by 20.0%. We show the visualization of embeddings from the encoder outputs for better observing the alignment across domain gaps. In Figure 4, it is observed that embeddings of rendered images and natural images have been aligned with samples from the 'chair' category in ShapeNet and Pix3D as source and target domain. Besides, we can see that the embeddings of the image and voxels from ShapeNet are well aligned in Figure 5 while the distribution of categories is kept properly.

Reconstruction for Pascal3D+ dataset. Similarly, none of the samples from Pascal3D+ has been shown up in the training stage. The common categories existing in both the Pascal3D+ and ShapeNet, 'aeroplane', 'car', 'chair' and 'tv monitor'. What is to be noticed is that we did not find any sample from 'table' that is mentioned in [39]. The natural images from the selected categories in ImageNet [10] are chosen as the target samples for the training procedure. The proposed LEM not only performs better on both CD and IoU, but also shows sound results on different categories in Table 2. No category label is involved during the training procedure. Our LEM shows robust reconstruction results for hard samples in Pascal3D+, especially when the scale of the object is small or the noise from the background largely affects the recognition of the target. In such cases, the baseline method crumbles in restoring the correct shape. Hence, the benefits of the SSA module of LEM are demonstrated. While for objects with shapes that are irregular compared to samples from the source domain the CSM module in our method helps to better map with the correct shape prior. With the above qualitative and quantitative experiments on two benchmarks, we can conclude that the proposed LEM authentically leads to a better semantic-level alignment between source and target domain, as well as generates high fidelity 3D reconstruction results.

4.2. Ablation and Analysis

Module ablation comparison. With the results of the ablation of the modules in Table 4, we can see that with the SSA module, the model performs better in extracting effective representation from the images and increase the baseline score of IoU from 0.241 to 0.266. Functioning with the module of CSM, the IoU is increased to 0.269 as the method leverages the semantic information and aligns the manifold of samples from the same category in both 2D

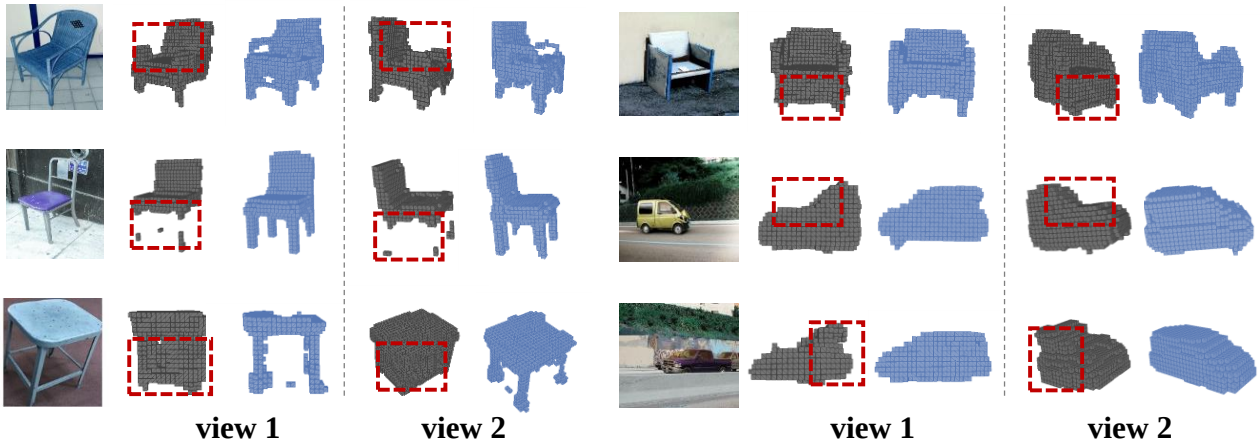

Figure 7. Reconstruction comparison of results generated by the DAREC and ours under two different camera views for some hard samples with different sizes and background noise. Our method better reconstruct these samples with robust structure and correct details.

Table 4. The ablation results on Pix3D under the single class setting showing the efficacy of each module in the proposed method.

Rec	Adv	SSA	CSM	IoU
✓				0.132
	✓			0.159
		✓		0.220
		✓	✓	0.237
✓		✓	✓	0.265
	✓	✓	✓	0.273
✓	✓	✓	✓	0.292

and 3D space. It is demonstrated the effectiveness of each module against the baseline method. Some visualization results for images from Pascal3D+ are shown in Figure 6. We can see that both the baseline and the proposed method succeed in reconstructing objects that are with common shapes and distinguishable from the background. However, for the hard sample with a complicated background, the baseline method tends to fail in recovering a proper shape and collapse in the details.

With different pooling scales in SSA, the performance varies and reaches the best when the number equals 64 with the balancing between the richness and compactness of the representation in the learned manifold. It is worth mentioning that during the evaluation, we found that the reconstruction results from the decoder pretrained on ShapeNet have an offset over the dataset with the ground truth of Pascal3D+. Therefore, we move the center of the generated voxel model to the center to keep align with the ground truth.

Effect of pooling scales. We further probe into the influence of the context features used in Figure.We choose context features at different stages $\{1, 2, 3, 4, 5\}$ from layers in the backbone network. The pooling sizes are chosen from $\{3, 6, 8\}$ to pool the context features into different scales. For each stage, we show the performance with three different combination of scales $\in \{3\}, \{3, 6\}, \{3, 6, 8\}$. It is proved that with multiple scales, the SSA can better assist the model to capture the local information from different levels. The best performance is achieved when the context feature is leveraged from the output of stage 4. It can be found that our LEM is robust to the loss term weights while the ratio between the CSM loss term and the adversarial loss term matters a little and the best ratio is $\beta : \lambda = 10 : 1$. Empirically, the model converges quickly and steadily when $\beta = 0.01, \lambda = 0.001$.

5. Conclusion

Inspired by the strong adaptability and generalization ability of human visual system in perceiving different 3D structures across various scenarios, we proposed to mimic such perception mechanism and accordingly stimulate with the proposed *"look, evolve and mold"* pivotal procedure. Incorporating the spatial structure with multi-scale pooling assists to distill the inherent knowledge and filter out those domain-sensitive background information. Thus, the desired shape can be 'mold' with the essential information acquired in the previous steps to reconstruct the stereo shape from the learned manifold. Nevertheless, there still exists disparity from the reconstruction results against the physical shapes with a large headroom to improve the expressiveness and flexibility in tackling diverse cases.

References

[1] Shai Ben-David, John Blitzer, Koby Crammer, and Fernando Pereira. Analysis of representations for domain adaptation. In *NIPS*, 2007. 2

[2] John Bridle. Probabilistic interpretation of feedforward classification network outputs, with relationships to statistical pattern recognition. *Neurocomputing: Algorithms, Architectures and Applications*, 1990. 6

[3] Jinkun Cao, Hongyang Tang, Hao-Shu Fang, Xiaoyong Shen, Cewu Lu, and Yu-Wing Tai. Cross-domain adaptation for animal pose estimation. In *Proceedings of the IEEE International Conference on Computer Vision*, pages 9498–9507, 2019. 2

[4] Angel X Chang, Thomas Funkhouser, Leonidas Guibas, Pat Hanrahan, Qixing Huang, Zimo Li, Silvio Savarese, Manolis Savva, Shuran Song, Hao Su, et al. Shapenet: An information-rich 3d model repository. *arXiv preprint arXiv:1512.03012*, 2015. 1, 6

[5] Xinyang Chen, Sinan Wang, Mingsheng Long, and Jianmin Wang. Transferability vs. discriminability: Batch spectral penalization for adversarial domain adaptation. In *International Conference on Machine Learning*, pages 1081–1090, 2019. 2

[6] Zhiqin Chen and Hao Zhang. Learning implicit fields for generative shape modeling. In *Proceedings of the IEEE Conference on Computer Vision and Pattern Recognition*, pages 5939–5948, 2019. 2

[7] Christopher B Choy, Danfei Xu, JunYoung Gwak, Kevin Chen, and Silvio Savarese. 3d-r2n2: A unified approach for single and multi-view 3d object reconstruction. In *European conference on computer vision*, pages 628–644. Springer, 2016. 1, 2

[8] Christopher Bongsoo Choy, Danfei Xu, JunYoung Gwak, Kevin Chen, and Silvio Savarese. 3d-r2n2: A unified approach for single and multi-view 3d object reconstruction. In *ECCV*, 2016. 1, 6, 7

[9] Carlo Colombo, Alberto Del Bimbo, and Federico Pernici. Metric 3d reconstruction and texture acquisition of surfaces of revolution from a single uncalibrated view. *IEEE transactions on pattern analysis and machine intelligence*, 27(1):99–114, 2005. 1

[10] Jia Deng, Wei Dong, Richard Socher, Li-Jia Li, Kai Li, and Li Fei-Fei. Imagenet: A large-scale hierarchical image database. In *CVPR*, 2009. 6, 7

[11] M. Everingham, L. Van Gool, C. K. I. Williams, J. Winn, and A. Zisserman. The PASCAL Visual Object Classes Challenge 2012 (VOC2012) Results. http://www.pascal-network.org/challenges/VOC/voc2012/workshop/index.html. 6

[12] Haoqiang Fan, Hao Su, and Leonidas J. Guibas. A point set generation network for 3d object reconstruction from a single image. In *Proceedings of the IEEE Conference on Computer Vision and Pattern Recognition (CVPR)*, July 2017. 2

[13] Haoqiang Fan, Hao Su, and Leonidas J. Guibas. A point set generation network for 3d object reconstruction from a single image. In *CVPR*, 2017. 6

[14] Qianyu Feng, Guoliang Kang, Hehe Fan, and Yi Yang. Attract or distract: Exploit the margin of open set. In *Proceedings of the IEEE International Conference on Computer Vision*, pages 7990–7999, 2019. 2

[15] Yasutaka Furukawa and Carlos Hernández. Multi-view stereo: A tutorial. *Foundations and Trends in Computer Graphics and Vision*, 2015. 1

[16] Yaroslav Ganin, Evgeniya Ustinova, Hana Ajakan, Pascal Germain, Hugo Larochelle, François Laviolette, Mario Marchand, and Victor S. Lempitsky. Domain-adversarial training of neural networks. *JMLR*, 2016. 5

[17] Rohit Girdhar, David F Fouhey, Mikel Rodriguez, and Abhinav Gupta. Learning a predictable and generative vector representation for objects. In *European Conference on Computer Vision*, pages 484–499. Springer, 2016. 1, 2

[18] Thibault Groueix, Matthew Fisher, Vladimir G. Kim, Bryan C. Russell, and Mathieu Aubry. Atlasnet: A papier-mâché approach to learning 3d surface generation. In *CVPR*, 2018. 6

[19] Thibault Groueix, Matthew Fisher, Vladimir G Kim, Bryan C Russell, and Mathieu Aubry. A papier-mâché approach to learning 3d surface generation. In *Proceedings of the IEEE conference on computer vision and pattern recognition*, pages 216–224, 2018. 2

[20] Peng Guan, Alexander Weiss, Alexandru O Balan, and Michael J Black. Estimating human shape and pose from a single image. In *2009 IEEE 12th International Conference on Computer Vision*, pages 1381–1388. IEEE, 2009. 1

[21] Erwan Guillou, Daniel Meneveaux, Eric Maisel, and Kadi Bouatouch. Using vanishing points for camera calibration and coarse 3d reconstruction from a single image. *The Visual Computer*, 16(7):396–410, 2000. 1

[22] Christian Häne, Shubham Tulsiani, and Jitendra Malik. Hierarchical surface prediction for 3d object reconstruction. In *2017 International Conference on 3D Vision (3DV)*, pages 412–420. IEEE, 2017. 2

[23] Kaiming He, Xiangyu Zhang, Shaoqing Ren, and Jian Sun. Spatial pyramid pooling in deep convolutional networks for visual recognition. *IEEE transactions on pattern analysis and machine intelligence*, 37(9):1904–1916, 2015. 4

[24] Kaiming He, Xiangyu Zhang, Shaoqing Ren, and Jian Sun. Deep residual learning for image recognition. In *CVPR*, 2016. 6

[25] Diederik P. Kingma and Jimmy Ba. Adam: A method for stochastic optimization. *ICLR*, 2014. 6

[26] Junnan Li, Pan Zhou, Caiming Xiong, Richard Socher, and Steven CH Hoi. Prototypical contrastive learning of unsupervised representations. *arXiv preprint arXiv:2005.04966*, 2020. 2

[27] Yunsheng Li, Lu Yuan, and Nuno Vasconcelos. Bidirectional learning for domain adaptation of semantic segmentation. In *Proceedings of the IEEE Conference on Computer Vision and Pattern Recognition*, pages 6936–6945, 2019. 2

[28] Jian Liang, Ran He, Zhenan Sun, and Tieniu Tan. Exploring uncertainty in pseudo-label guided unsupervised domain adaptation. *Pattern Recognition*, 96:106996, 2019. 2

[29] Tsung-Yi Lin, Piotr Dollár, Ross Girshick, Kaiming He, Bharath Hariharan, and Serge Belongie. Feature pyramid networks for object detection. In *Proceedings of the IEEE conference on computer vision and pattern recognition*, pages 2117–2125, 2017. 4

[30] Mingsheng Long, Yue Cao, Zhangjie Cao, Jianmin Wang, and Michael I Jordan. Transferable representation learning with deep adaptation networks. *IEEE transactions on pattern analysis and machine intelligence*, 41(12):3071–3085, 2018. 2

[31] Mingsheng Long, Yue Cao, Jianmin Wang, and Michael Jordan. Learning transferable features with deep adaptation networks. In *International conference on machine learning*, pages 97–105. PMLR, 2015. 2

[32] Yawei Luo, Ping Liu, Tao Guan, Junqing Yu, and Yi Yang. Significance-aware information bottleneck for domain adaptive semantic segmentation. In *Proceedings of the IEEE International Conference on Computer Vision*, pages 6778–6787, 2019. 2

[33] Yawei Luo, Ping Liu, Tao Guan, Junqing Yu, and Yi Yang. Adversarial style mining for one-shot unsupervised domain adaptation. *arXiv preprint arXiv:2004.06042*, 2020. 2

[34] Yawei Luo, Liang Zheng, Tao Guan, Junqing Yu, and Yi Yang. Taking a closer look at domain shift: Category-level adversaries for semantics consistent domain adaptation. In *Proceedings of the IEEE Conference on Computer Vision and Pattern Recognition*, pages 2507–2516, 2019. 2

[35] Priyanka Mandikal, KL Navaneet, Mayank Agarwal, and R Venkatesh Babu. 3d-lmnet: Latent embedding matching for accurate and diverse 3d point cloud reconstruction from a single image. *arXiv preprint arXiv:1807.07796*, 2018. 2

[36] Lars Mescheder, Michael Oechsle, Michael Niemeyer, Sebastian Nowozin, and Andreas Geiger. Occupancy networks: Learning 3d reconstruction in function space. In *Proceedings of the IEEE Conference on Computer Vision and Pattern Recognition*, pages 4460–4470, 2019. 1, 2

[37] Vinod Nair and Geoffrey E. Hinton. Rectified linear units improve restricted boltzmann machines. In *ICML*, 2010. 6

[38] Jeong Joon Park, Peter Florence, Julian Straub, Richard Newcombe, and Steven Lovegrove. Deepsdf: Learning continuous signed distance functions for shape representation. In *Proceedings of the IEEE Conference on Computer Vision and Pattern Recognition*, pages 165–174, 2019. 1, 2

[39] Pedro O Pinheiro, Negar Rostamzadeh, and Sungjin Ahn. Domain-adaptive single-view 3d reconstruction. In *Proceedings of the IEEE International Conference on Computer Vision*, pages 7638–7647, 2019. 2, 6, 7

[40] Can Qin, Haoxuan You, Lichen Wang, C-C Jay Kuo, and Yun Fu. Pointdan: A multi-scale 3d domain adaption network for point cloud representation. In *Advances in Neural Information Processing Systems*, pages 7192–7203, 2019. 2

[41] Christos Sakaridis, Dengxin Dai, and Luc Van Gool. Guided curriculum model adaptation and uncertainty-aware evaluation for semantic nighttime image segmentation. In *Proceedings of the IEEE International Conference on Computer Vision*, pages 7374–7383, 2019. 2

[42] Peng Su, Shixiang Tang, Peng Gao, Di Qiu, Ni Zhao, and Xiaogang Wang. Gradient regularized contrastive learning for continual domain adaptation. *arXiv preprint arXiv:2007.12942*, 2020. 2

[43] Xingyuan Sun, Jiajun Wu, Xiuming Zhang, Zhoutong Zhang, Chengkai Zhang, Tianfan Xue, Joshua B Tenenbaum, and William T Freeman. Pix3d: Dataset and methods for single-image 3d shape modeling. In *Proceedings of the IEEE Conference on Computer Vision and Pattern Recognition*, pages 2974–2983, 2018. 6, 7

[44] Maxim Tatarchenko, Alexey Dosovitskiy, and Thomas Brox. Octree generating networks: Efficient convolutional architectures for high-resolution 3d outputs. In *Proceedings of the IEEE International Conference on Computer Vision*, pages 2088–2096, 2017. 2, 7

[45] Shubham Tulsiani, Tinghui Zhou, Alexei A. Efros, and Jitendra Malik. Multi-view supervision for single-view reconstruction via differentiable ray consistency. In *CVPR*, 2017. 6, 7

[46] Eric Tzeng, Judy Hoffman, Kate Saenko, and Trevor Darrell. Adversarial discriminative domain adaptation. In *Proceedings of the IEEE conference on computer vision and pattern recognition*, pages 7167–7176, 2017. 2

[47] Qian Wang and Toby Breckon. Unsupervised domain adaptation via structured prediction based selective pseudo-labeling. In *Proceedings of the AAAI Conference on Artificial Intelligence*, 2020. 2

[48] Xiaolong Wang, Ross Girshick, Abhinav Gupta, and Kaiming He. Non-local neural networks. In *Proceedings of the IEEE conference on computer vision and pattern recognition*, pages 7794–7803, 2018. 4

[49] Jiajun Wu, Yifan Wang, Tianfan Xue, Xingyuan Sun, Bill Freeman, and Josh Tenenbaum. Marrnet: 3d shape reconstruction via 2.5d sketches. In *NIPS*, 2017. 6

[50] Jiajun Wu, Chengkai Zhang, Tianfan Xue, Bill Freeman, and Josh Tenenbaum. Learning a probabilistic latent space of object shapes via 3d generative-adversarial modeling. In *Advances in neural information processing systems*, pages 82–90, 2016. 1, 2

[51] Jiajun Wu, Chengkai Zhang, Tianfan Xue, Bill Freeman, and Josh Tenenbaum. Learning a probabilistic latent space of object shapes via 3d generative-adversarial modeling. In *NIPS*, 2016. 6

[52] Jiajun Wu, Chengkai Zhang, Xiuming Zhang, Zhoutong Zhang, William T. Freeman, and Joshua B. Tenenbaum. Learning shape priors for single-view 3d completion and reconstruction. In *ECCV*, 2018. 6, 7

[53] Yu Xiang, Roozbeh Mottaghi, and Silvio Savarese. Beyond pascal: A benchmark for 3d object detection in the wild. In *IEEE winter conference on applications of computer vision*, pages 75–82. IEEE, 2014. 6

[54] Haozhe Xie, Hongxun Yao, Xiaoshuai Sun, Shangchen Zhou, and Shengping Zhang. Pix2vox: Context-aware 3d reconstruction from single and multi-view images. In *Proceedings of the IEEE International Conference on Computer Vision*, pages 2690–2698, 2019. 2

[55] Qiangeng Xu, Weiyue Wang, Duygu Ceylan, Radomir Mech, and Ulrich Neumann. Disn: Deep implicit surface network for high-quality single-view 3d reconstruction. In *Advances in Neural Information Processing Systems*, pages 492–502, 2019. 2

[56] Yang Zou, Zhiding Yu, Xiaofeng Liu, BVK Kumar, and Jinsong Wang. Confidence regularized self-training. In *Pro-*

ceedings of the IEEE International Conference on Computer Vision, pages 5982–5991, 2019. 2